




Multi-objective Sizing of a Standalone Renewable Power System for Offshore Oil and Gas Applications

Ahmad M. Saber^{*‡}, T. A. Boghdady^{**}, Doaa K. Ibrahim^{**}

^{*}EECS Department, Faculty of Engineering, Khalifa University, Abu Dhabi 127788 UAE

^{**}Department of Electrical Power Engineering, Faculty of Engineering, Cairo University, Giza 12613 Egypt

(ahmad.m.saber@ieeee.org, Engtarek82@cu.edu.eg, doaakhalil73@eng.cu.edu.eg)

[‡]Corresponding Author; T. A. Boghdady, Department of Electrical Power Engineering, Faculty of Engineering, Cairo University, Giza 12613 Egypt, Tel: +201020443386, Engtarek82@cu.edu.eg

Received: 12.10.2021 Accepted: 03.11.2021

Abstract- The potential of electrifying Offshore Oil and Gas platforms by Hybrid Renewable Energy Sources (HRESs) was paid attention to recently. As sensitive loads, these installations require a high level of reliability, which requires special consideration in modeling. This load sensitivity contradicts the intermittent nature of HRESs like winds and waves. Implementing batteries in a similar energy system could help decrease the variation in the generated power. However, practical batteries are known to degrade over many factors. In this article, a study is presented on quantifying the enhancement in the reliability of supply caused by coupling of a Wind-Wave (WW) hybrid offshore energy converter (named: HOEC) unit with a Lithium-Based Energy Storage System (LBESS), while considering LBESS's degradation and load sensitivity, and optimizing the battery size and WW ratios. The optimization is solved using a semi-analytical approach and compared against two heuristic algorithms, which are particle swarm optimization and pattern search algorithm. Results demonstrate possible system reliability enhancement while optimizing the system designed using the proposed approach.

Keywords Hybrid renewable energy systems, wind energy, wave energy, energy storage, lithium-ion battery, Offshore installations.

1. Introduction

The Offshore Oil and Gas (OOnG) sector is the foundation to many economies. OOnG platforms are massive structures installed worldwide. They are typically in various water depths and at different distances from the shore. It is no secret that OOnG installations account for a great amount of the Greenhouse Gases (GHG) emissions [1–4]. A key solution to this problem could be the direct electrification of these platforms [5, 6]. Nowadays, there are ongoing projects on the electrification of OOnG platforms in the North and Norwegian Seas, beside the ones electrified already [6]. An alternative is making use of offshore clean energy sources [7 – 9]. Major OOnG companies like Equinor, Shell and Eni producers have started renewables businesses already [10 – 12]. Since offshore wind industry initially learnt a lot from OOnG industry, OOnG could benefit from offshore renewables in return [13]. Offshore wind energy has one of the highest impacts on GHG emission reduction. Therefore, the thought of using offshore wind energy to supply OOnG platforms occurred to many researchers [2, 8, 9, 13]. What is more is, recently, authors of [14] advocated the exploration of another

ocean renewable source, wave energy, for supplying OOnG platforms. Consequently, we could benefit from generating power from more than one renewable energy source to improve their competitiveness, following similar applications as proposed in [15–21].

1.1 Renewables for OOnG

In [22], the integration of 20 MW wind power was assessed in terms of fuel consumption savings and reductions in CO₂/NO_x. Moreover, authors have studied 9 simulations for the grid stability after wind power integration. Then the simulations have been compared to identify the optimum amount of wind power output for integration. A case study on five interconnected OOnG platforms and a wind farm of 100 MW was conducted in [23]. A case study was carried out on wind power integration and without it, to compare the results. The results were 21% to 30% reduction in the fuel consumption, subject to the operational strategy of gas turbines. Simulations were also done for reduction in CO₂/NO_x emissions. In [24], the wind energy was integrated to reduce GHG emissions, where wind farm technology was

connected with different platforms. The system model consisted of 5 OOnG platforms connected to 100 MW offshore Wave Energy Converters (WETs) farm. Each platform has two gas turbines working in parallel. Moreover, two operational strategies were investigated for the gas turbines. Results were 21-33% reduction in GHG emissions. The exploration of WECs' potential to be connected with OOnG platforms has not been done rigorously yet. Authors of [25] have concluded that offshore wind energy is the best alternative for delivering power to the OOnG platforms. The work presented numerical simulations for emissions reduction and fuel saving. It was stated that the operational strategy should be wisely chosen for getting stable and economic operation. The work also presented wind farms working in parallel with gas turbines with 40% wind energy share. Two operational strategies were investigated: one for load sharing and another start/stop strategy where one turbine is shut down.

Due to the strong correlation between winds and ocean waves, they have been candidates for a combination. The simplest way is co-locating WETs and WECs. This method was rigorously presented in the literature [8, 20, 26], for similar applications to OOnG loads. Authors in [26] have studied the allocation of several WECs on a floating platform from a hydrodynamic point of view. Through case studies in different European cities, the benefits of combining offshore wind and wave energies is reaching a less variable supply, but with no battery option. "WindWec" is a device concept introduced in [21] that was inspired by the success of offshore floating WETs and Wave Star WEC [27]. It was concluded that wave converters help reducing the structural loads caused by the waves on the turbine's structure, while the turbine structurally supports the converter.

1.2 Energy Storage for OOnG

Despite the improvement in the power output of the combined wind-wave device compared to separate WETs or WECs, it is still of low reliability. For the problems under study, several works integrated energy storage units to the energy system such as [26-31]. Researchers at Equinor recently proposed Bat-Wind concept [32]. It makes use of the turbine's body to install the battery packs along its body. An alternative could be placing them on the WEC's body.

The main advantages of integrating energy storage with OOnG system supplied by renewable energy can be summarized as: (i) increased generation reliability and security, (ii) minimized the necessary installed capacity of wind and wave energies, and (iii) improved stability of the power system.

Nevertheless, the battery models used in previous literature were all generic and fail to account for battery degradation, which may delay the process of commercializing the idea. In [33], an approach for including battery degradation in the sizing problem was presented; however, this model could be improved to include more of the factors that collaborate in practical battery degradation: calendar and cyclic.

Lithium-ion (Li-ion) batteries are emerging rapidly, due to their high energy and power densities as well as maturity in manufacturing [22-27]. Their utilization in large renewable energy systems was previously investigated. The first

commercial lithium ion batteries were produced by Sony in 1990. Since then, improved material developments have led to vast improvements in terms of the energy density (increased from 75 to 200 Wh/kg) and cycle life (increased to as high as 10,000 cycles). Among all energy storage technologies, lithium-based battery energy storage system (LBESS) was selected in this research to represent the energy storage element due to its various advantages [34, 35].

1.3 Paper Contribution

In this research, we build on the previous work in renewable energy sizing and planning literature. We cover an untapped area by investigating the effect of coupling a HOEC with LBESS on the supply continuity for an OOnG load, over a year-long period time, considering: (i) Battery fading, and (ii) Load sensitivity. A case study with different scenarios was carried out using real measured data of an OOnG platform. Generation mixes covered several WW ratios. Optimal battery sizes were obtained in each scenario. Finally, all results were analyzed. All the simulation was carried out in MATLAB environment.

The rest of the article consists of 4 sections. Section 2 covers the modeling aspects of the system and its different components. Next, Section 3 presents the problem formulation and the results are fully discussed in Section 4. Finally, the conclusion comes in handy in Section 5.

2. System Modelling

The feeding system, the OOnG load and the energy management will be discussed and modelled as follows:

2.1. Wave Energy Converter

Several wave-energy converting techniques exist today. Among them, Wave-star [36] is selected as for its scalability and suitability for a synergy with WETs. Furthermore, there are available power matrices based on data from WECs already installed in several locations [37]. The generator machine is based on rows of floats which are all fixed by leavers to a horizontal shaft, with one-way bearings. The slowly revolving shafts are connected through a gearbox to a generator, like the method used in a wind turbine. The length of the row of floats is at least a wavelength. When a wave passes, the first float is lifted upwards, because of the buoyancy, and the lever locks onto the shaft, when the speed exceeds the revolving speed of the shaft. This generates a torque to the shaft. When the wave descends, the grip of the shaft is loosened, and the float moves freely down to a lower position until the next wave appears. The next float in line, adds a similar torque to the shaft. The shaft in this way integrates the torque from all upward moving floats at a fixed rotational speed – a speed that is determined by the gearing and the generator speed.

In contrary to linear wave energy converting mechanisms, the power produced by a certain Wave-star WEC (P_{WAVE}) is non-linear. It can be modelled by a 2D matrix, incorporating significant wave height (H_s), and average wave period (T_w) as inputs. H_s is the average wave height (trough to crest) of the

one-third highest waves. H_s is the most important parameter for characterization of the statistical distribution of ocean waves, and it is the parameter most often given in weather forecasts. The production from the Wave Star prototype depends strongly on H_s . In this piece of work, the four Wave-star models published in [38, 39] were studied. The models are summarized in Table 1.

Table 1. WEC models and their power ratings

WEC Model	Nominal Power (MW)
Wave-star C	1
Wave-star E	2
Wave-star H	4
Wave-star K	15

For demonstration, Wave-star C, of 1 MW nominal power, consists of 20 floats, each of a 6 m diameter and 12-meter arm length. The device is of a power take off efficiency equals 0.9. Power production starts at $1.5 T_w$. The maximum power production by this WEC is achieved at $4.5 T_w$ and $2.25 H_s$, or, $3.5 T_w$ and $2.75 H_s$, and continues with the increase of H_s up to $3.5 H_s$, beyond which the storm protection is applied. For the same H_s , P_{WAVE} increases directly with the increase in T_w until a certain limit of T_w (9.5 to 12.5 sec for model C, for example). Beyond this limit, P_{WAVE} decreases instead of increasing. This reduction is a result of changed settings in the Power-Take-Out system currently implemented.

2.2. Wind Energy Converter

Wind power (P_{WIND}) was modelled by the WET’s power curve. In this sense, P_{WIND} directly depends on the wind speeds (WSPDs). Therefore, WSPDs were re-calculated and referred to the turbine’s hub height using the following well-known relation:

$$\frac{v_1}{v_2} = \left(\frac{h_1}{h_2}\right)^z \quad (1)$$

Where v_1 and v_2 are wind velocities at heights h_1 and h_2 , respectively. The value of 0.11 is chosen for the friction coefficient z , according to [33], it was empirically determined to be applicable most of the time over the ocean.

P_{WIND} is modelled as follows:

$$P_{WIND}(t) = \begin{cases} P_N & v_n \leq v(t) \leq v_{max} \\ (a \times v^b(t) + c)P_N & v_{min} \leq v(t) \leq v_n \\ 0 & otherwise \end{cases} \quad (2)$$

where $P_{WIND}(t)$ is the electric power generated by the wind turbine at time t , P_N is the nominal power of the turbine, v_{min} is the cut-in speed of the wind turbine, v_n is the nominal speed of the turbine and v_{max} is the cut-out speed of the wind turbine. The constants a , b and c are determined for each turbine separately by curve-fitting and interpolating each turbine’s power curve data.

In simulation, all the technical data were drawn from the manufacturers’ datasheets. WSPDs were corrected for corresponding heights under investigation using Equation (1).

Two different large-sized commercially available floating WETs, as shown in Table 2, were selected in this research. 9.5 MW is approximately the largest nominal power in the available offshore WETs today, after the 10 MW Siemens WET. The WETs were chosen of different maximum power to enable different WW ratios in the study. Both WETs share a v_n of approximately 14 m/s. In addition, they are characterized by v_{min} and v_{max} of nearly 3 and 25 m/s, respectively.

Table 2. WET models characteristics

WET Model	SWT-2.3-93	V164-9.5
Manufacturer	Siemens	Vestas
P_N (MW)	2.3	9.5
Hub height (m)	80	130
v_{max}	3.5	3
v_n	14	14
v_{min}	25	25

2.3. LBESS

Lithium-ion batteries are emerging rapidly, due to their high energy and power densities as well as maturity in manufacturing [39-42]. Their utilization in large renewable energy systems was previously investigated. Among different Li-ion chemistries, Lithium-iron-phosphate/graphite (LFP/C) was the selected battery chemistry following [41]. It was foreseen to suite our proposed application as it was tested for a large-scale energy application. LBESS is modelled by its state of charge (SOC) and produced power (P_{BAT}). Each LBESS has a nominal capacity (C_O) and nominal power capability (P_{BO}) at ($t=0$) or the time of installation. In our problem, as the resolution (Res) of the available data is one hour, P_{BO} is defined as the power the LBESS can deliver over one hour. Accordingly, absolute values of P_{BO} cannot be greater than C_O , as absolute values. Inside LBESS, the charging process is presumed to be identical to the discharging, but in the opposite direction. The charging efficiency is anticipated to be 0.95. LBESS’s depth of discharge (DoD) was set to 0.8. For all instants, the following two constrains must be satisfied:

$$SOC_{MIN} \leq SOC(t) \leq SOC_{MAX}(t) \quad (3)$$

$$P_{Bat_MIN}(t) \leq P_{Bat}(t) \leq P_{Bat_MAX}(t) \quad (4)$$

where SOC_{MIN} and SOC_{MAX} are the minimum and maximum SOC limits, respectively, while P_{Bat_MIN} and P_{Bat_MAX} are the minimum and maximum limits of P_{Ba} . To account for LBESS degradation, equations (5)–(8) [41] were fused with the LBESS model.

$$C_{fade_cal} = 1.9775 \times 10^{-11} \times e^{0.07511 T(t)} \times 1.639 \times e^{0.007388 SOC(t)} \times t^{0.8} \quad (5)$$

$$PC_{fade_cal} = 1.075 \times 10^{-10} \times e^{0.06995 T(t)} \times 0.02672 \times SOC(t)^{0.4513} \times t \quad (6)$$

$$C_{fade_cyc} = 2.6418 e^{-0.01943 SOC(t)} \times 0.004 e^{0.01705 T(t)} \times 0.0123 cd(t)^{0.7162} \times nc(t)^{0.5} \quad (7)$$

$$PC_{fade_cyc} = 2.0947 \times 10^{-7} \times e^{0.04759 T(t)} \times 3.853 \times 10^{-6} \times cd(t)^{0.7891} \times nc(t) \quad (8)$$

Where the degradation factors are time (t), number of cycles (nc), temperature (T), SOC and cycle depth (cd). Capacity fade (C_{fade}) is the maximum of LBESS capacity's: calendar fade (C_{fade_cal}) and cyclic fade (C_{fade_cyc}) at any moment. LBESS's power capability fade (PC_{fade}) is the larger of both its cyclic (PC_{fade_cyc}) and calendar (PC_{fade_cal}) fades at any time. The LBESS's end of life (EOL) criterion was defined as 20% capacity fading [41]. This model was preferred for being more practical, as it was concluded from an accelerated ageing study. Furthermore, it is thought to account for most ageing factors.

2.4. Load, and Reliability Index

Load power (P_L) was modelled as a constant continuous load, to represent the critical load. Equivalent Loss Factor (ELF) index was chosen as the reliability constraint [43]:

$$ELF = \frac{1}{H} \times \sum_{t=1}^H \frac{L(t)}{P_L(t)} \quad (9)$$

where L is, the loss of power at hour (t) and H is the total number of hours in the year. ELF is a function of the supplied power from the HRESs and LBESS, the load level and time; hence, it reflects the overall system's reliability. At any instance ELF must not exceed the limit of 0.1 [42].

2.5. Energy Management of the System

As a step on the WW device synergy, the energy generation system is modelled as a combined one WET and one WEC system; being referred to as WW-HOEC from now on. If an LBESS is included, it will be denoted as WWB-HOEC (Wind-Wave-Battery HOEC). Fig. 1 shows the system under study, which is similar to that in [43–46]. Wind and wave power generators generate electricity from the oceans' wind and wave motion. Battery charges when there is excess of electricity generation and supports the load when the generation is low. The OonG platform is the AC load, connected through a DC/AC converter. Dump load consumes the excess energy when both the load and the battery are satisfied. The system inverter's efficiency is 0.95. For a wider analysis, it was necessary to study different wind-to-wave ratios in the WW-HOEC—these are different WET-WEC combinations forming systems with a variety of nominal powers, where P_o is the rated power of the system. Subsequently, all the combinations between the aforementioned WETs and WECs in Tables 1 and 2 were used to form "WW-HOEC models", which are shown in Table 3, and Fig. 2.

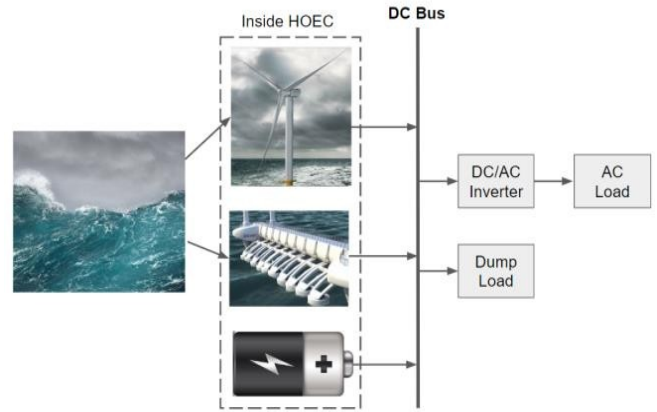


Fig. 1. The hybrid renewable energy system under study

Table 3. WW-HOEC models and their characteristics

HOEC Model	WW Powers Ratio	P_o (MW)
A	2.3: 1	3.3
B	2.3: 2	4.3
C	2.3: 4	6.3
D	2.3: 15	17.3
E	9.5: 1	10.5
F	9.5: 2	11.5
G	9.5: 4	13.5
H	9.5: 15	24.5

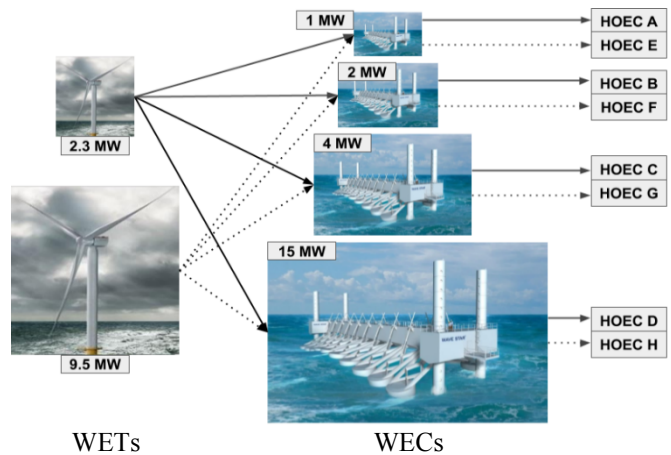


Fig. 2. Formulation of HOECs mentioned in Table 3.

As P_{HOEC} is the output power from a WW-HOEC, the following two equations hold up well:

$$P_{REN}(t) = P_{WIND}(t) + P_{WAVE}(t) \quad (10)$$

$$P_{HOEC}(t) = P_{REN}(t) + P_{Bat}(t) \quad (11)$$

Regarding the power flow of the generated power P_{REN} , the highest priority is given for satisfying P_L , followed by charging LBESS, after that closing the line to the dump load. This philosophy results in 5 possible states at any time:

- a. $P_{REN}(t) = P_L$
- b. $P_{REN}(t) > P_L$ & $SOC_{MAX}(t) > SOC(t) \geq SOC_{MIN}$

- c. $P_{REN}(t) > P_L$ & $SOC_{MAX}(t) = SOC(t)$
- d. $P_{REN}(t) < P_L$ & $SOC_{MAX}(t) \geq SOC(t) > SOC_{MIN}$
- e. $P_{REN}(t) < P_L$ & $SOC(t) = SOC_{MIN}$

where in state a, P_{REN} will neither be supplied to LBESS nor drawn from it, and all the energy will be used to fulfil P_L . LBESS will charge in state b, and discharge in stated. Alternatively, in state c, the extra energy will be directed to the dump load; while there will be some load loss in state e, and only in this state will $L(t)$ have a value. It is worth noticing that in a grid-connected system, the dump load will be replaced by the connection with the grid. Hence, the dumped energy will be utilized by the grid.

3. Problem Formulation

The problem was formulated as a multi-objective optimization problem and solved using a formulated heuristic algorithm which is presented in Fig. 3. To demonstrate HOEC’s performance as well as the improvement caused by integrating the LBESS, three values were to be found while maintaining the reliability condition:

- i. P_L1 : Maximum P_L , that a WW-HOEC can satisfy.
- ii. P_L2 : Maximum P_L , that a WWB-HOEC can satisfy.

Optimum LBESS size for (ii): C_O and P_{BO} .

3.1. Before Integrating the LBESS: Maximizing P_L1

To find this value, algorithm 1 was designed (shown in Fig. 3: part 1). As illustrated, it is a simple semi-analytical-semi-iterative optimization that is characterized, in addition, by accuracy.

$$\text{Objective1: } \max(P_L) = P_L1 \quad (12)$$

As P_L1 cannot be of a negative value, the starting value of P_L is zero. At the same time, a “Maximum Res” value is set, while the starting Res value is set to unity. The Res is the reciprocal of ΔP_L , which is the incremental step of P_L1 . After the increment, the constraint ELF is calculated using equation (9) and compared to the tolerable ELF_{MAX} as explained in section II D. Depending on the previous step, the optimization sequence either enters a new loop of increment or decrement to the current value of P_L by ΔP_L . Next, if Maximum Res is not reached, the Res is upgraded. The new Res is always ten times the older one. If Maximum Res is reached, then the current value of P_L1 is the desired maximum value.

3.2. After Integrating the LBESS: Maximizing P_L2 while Minimizing C_O and P_{BO}

The improvement caused after integrating LBESS can be known by determining P_L2 and optimum C_O and P_{BO} . The objectives of this multi-objective optimization are:

$$\text{Objective2: } \max(P_L) = P_L2 \quad (13)$$

$$\text{Objective3: } \min(C) = C_O \quad (14)$$

$$\text{Objective4: } \min(P_B) = P_{BO} \quad (15)$$

For more simplicity, the objectives were analytically split into two steps: finding P_L2 , and optimal sizing of LBESS.

1) Finding P_L2

The logic behind this part is that incorporating LBESS in a HOEC, should allow an increase in the level of possible P_L to be satisfied, under the same level of P_{REN} and same constraints. Initially, the value of P_L is set to P_L1 , as found in 3.1, and the objective is as described in Equation (13). Three new unknowns appear here: C_S , ELFs and ELF_{MIN} . Firstly, C_S is a vector of increasing LBESS’ C_O , ranging from 0 MWh to UL times P_O the of the system; with UL being the upper limit of C_S . Secondly, ELFs is a current optimization. Steps of this search algorithm are illustrated in Fig. 3: part 2.

2) Optima LBESS Sizing for P_L2

By the optimal sizing of LBESS, we mean to optimally size both its C_O and P_{BO} . Therefore, this is done in two stages:

Stage 1: Finding C_O

The value of C (in C_S) corresponded to P_L2 is taken as a starting point. Initially, P_B is set equal to C since it cannot be greater than it in our problem. In each iteration, the values of C_O and P_{BO} are decremented by the set Res, and the constraint is evaluated. The sequence continues, as in Fig. 3: part 3, until C_O (optimum value of C) is reached.

Stage 2: Finding P_{BO}

It is the only remaining value to determine. The starting value of P_B is set to that of C_O . Then it decreases and the constraint is evaluated, similar to the previous sequences. P_{BO} (Optimum P_B) is the output of the algorithm in Fig. 3: part 4.

4. Simulation Results

The main scope of the simulations is to investigate which combination of WET-WEC-LBESS is the best candidate in terms of power production, to become a single HOEC device.

For each combination, the simulation tried to maximize the load supplied continuously, while optimizing the LBESS parameters. To do this comparison, a case study was performed using different scenarios (numbered 1-8) to resemble applying eight different HOEC models (denoted by A-H), covering all combinations of used WETs and WECs. Standard meteorological for Louisiana OonG port at 27 km from the shore were obtained. For each generation mix as, problems described in the previous Section were solved. All simulation work was developed in MATLAB workspace environment. The obtained results are threefold: customer-side or results, P_L generation results represented by Capacity factor (CF), and finally LBESS results. Table 4 shows the P_L results obtained in the case study. P_L1 is P_L for WW-HOEC without LBESS, while P_L2 is that of WWB-HOEC.

Table 4. Case study maximum load results

Scenario	HOEC Model	P_L1 (MW)	P_L2 (MW)
1	A	0.4544	0.5286
2	B	0.5244	0.6034
3	C	0.772	0.968
4	D	1.4866	1.6473
5	E	0.7293	0.9696
6	F	0.8304	1.086
7	G	1.3973	1.7293
8	H	2.2162	2.4833

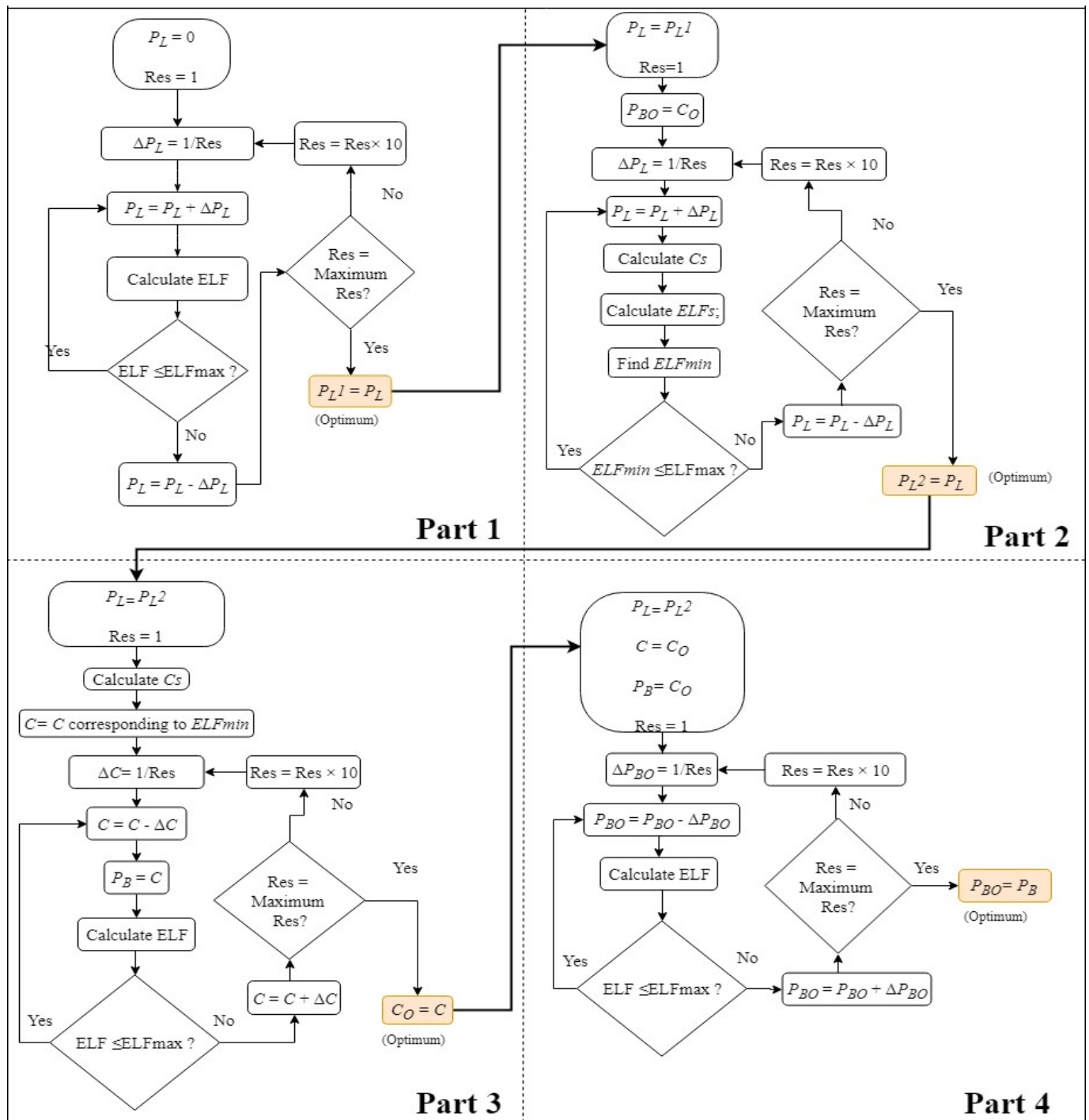


Fig. 3. The complete sizing sequence, part 1: maximizing P_{L1} ; part 2: maximizing P_{L2} ; part 3: optimum C_o ; part 4: optimum P_{Bo} .

For better analysis, two new factors were defined. They are δ and φ which stand for (P_{L1}/P_o) and (P_{L2}/P_o) ratios, respectively. In Fig. 4, a comparison between δ and φ is illustrated. It can be noted that integrating LBESS into WW-HOEC allowed higher P_L to be satisfied. The increase in the load level, measured by $(\varphi-\delta)$, ranged from 0.93 to 3.11%. The highest δ and φ ratios were associated with the utilization of HOEC models: A and C. The highest δ was found to be: 13.77% for HOEC-A, followed by 12.25% for HOEC-C, while φ values were 16.02% and 15.37% for the same models.

When it comes to CFs, Fig. 5 shows the values for each case. Being able to achieve nearly 40% CF, model C seems to be the fittest to implement. In the second place comes model A with about 36% CF, which is about 12% more than the smallest CF occurring with model D. It can be noted that the trend says higher WW ratios do not necessarily exhibited better generation performances. At this point models A and C of WW- HOEC show the best performances from the points of view of the generation and the load.

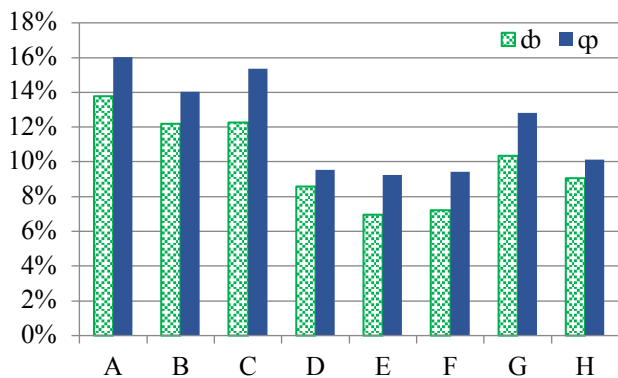


Fig. 4. HOEC models δb and ϕ ratios

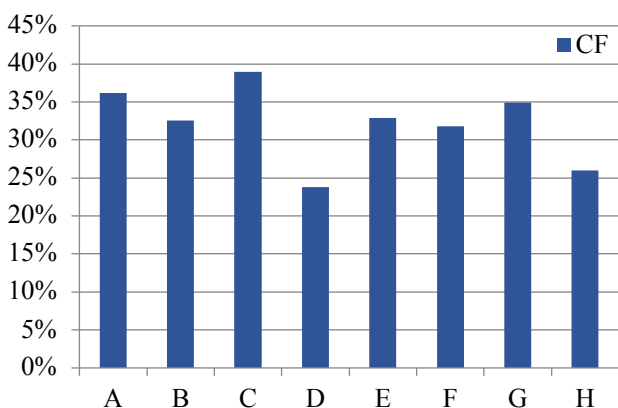


Fig. 5. HOEC models' CF values.

Next, a comparison between LBESS sizes is shown below in Fig. 6. As illustrated, even though C_o values are larger than usual in offshore applications (7.3 MWh and larger), this issue could be handled if additional constraints are included in the optimization problem, in future research. Besides, it can be noted that Model A required the smallest C_o and P_{BO} sizes among all the models, with values of 7.3 MWh and 1.4677 MW, respectively. Hence it is of a good candidacy for being the reference model in future commercial scale. Moreover, the effect of LBESS degradation represented by LBESS's C_{fade} percentage per year and corresponding lifetimes are shown in Fig. 7. These quantities mean LBESS would be typically changed 6 times in a 25-years project. Finally, a summary of the LBESS parameters' results is provided in Table 5.

Table 5. Case study results

Scenario	HOEC Model	C_o (MWh)	P_{BO} (MW)	Annual C_{fade} (%)	LBESS Lifetime (years)
1	A	7.3	1.4677	5.13	3.9
2	B	9.5591	1.4358	5.16	3.87
3	C	17.0081	2.6529	5.41	3.69
4	D	21.4343	7.1217	5.21	3.84
5	E	21.6586	4.0749	5.02	3.98
6	F	24.1554	4.6823	4.88	4.09
7	G	30.2794	6.4187	5.18	3.86
8	H	35.3523	13.6818	5.22	3.83

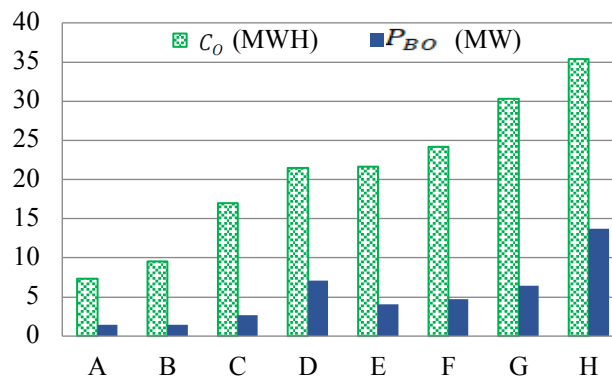
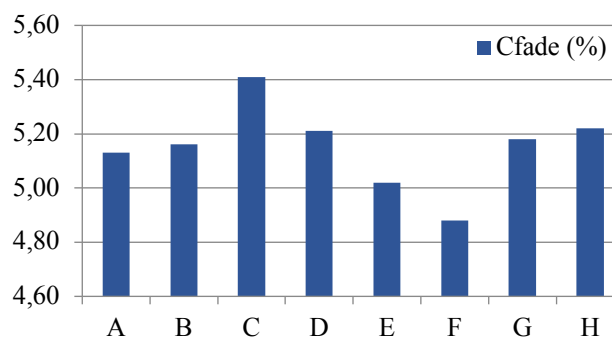
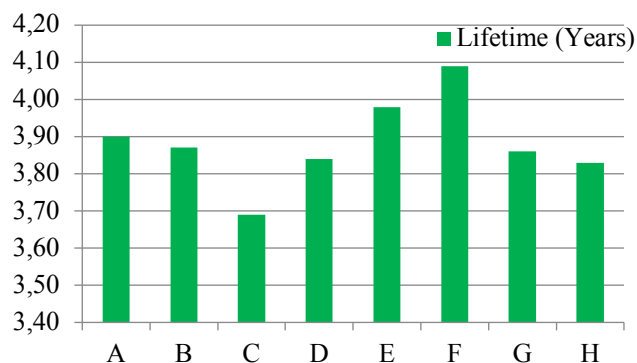


Fig. 6. WWB-HOEC models and LBESS sizes: C_o in (MWh) and P_{BO} in (MW).



(a)



(b)

Fig. 7. LBESS degradation: (a) C_{fade} per year (%), and (b) LBESS Lifetime in years.

The performance of HOEC A, for a complete year, is illustrated in Fig. 8-Fig. 10. In Fig. 8, the power generated from each source (Fig. 8-a and b) and the power-production performance of the LBESS (Fig. 8-c) are drawn for one year. While the graph in Fig. 9-a illustrates the curve of the combined generated powers by both the WET and WEC. Actually, the power generation reaches the maximum of both WET and the WEC several times, while the minimum generation is about 0.1 MW. Power production almost does not stop, except for a few hours, throughout the year. In the interval of hours from 1 to 3000 -which corresponds to months January to early May-, and hours 6500 to the end of the year -accounting for the typical autumn season-, the power production from HOEC was at its highest value. Nevertheless, the CF in the latter period was, apparently, lower than that of the former; with the CF being the

ratio between the actual energy produced by HOEC in total over a specific period of time to the maximum possible energy output over the same period. During a wintery high- energy day, power production would reach the peak several times (illustrated in Fig. 9-b). The period of hours from 3500 to 6000 was of a lower energy production, which is the expected for summery weather with lower wind speeds and waves, and steadier power production. Fig. 9-c shows an example of a summer day with a relatively low energy production.

Moving on, the behaviour of LBESS, in the same case study, is demonstrated in Fig. 10. A slow but steady decrease in the LBESS’s maximum SOC can be seen in Fig. 10-a, with the LBESS exerting fewer number cycles in the summertime. This goes in line with the previous observation that the power production was lower at this period. Parts b and c in Fig. 10 show a highly varying increase in the C_{fade} and PC_{fade} percentages, respectively, all over the year, with a noticeable rapid increase during the hottest period of the year. This is a clear illustration of the synergy between all the participating factors in the LBESS degradation process. Subsequently, for a typical 25-years project, considering the LBESS EOL criterion, replacement of the LBESS would be needed 6 times during the project—considering even meteorological behaviour for all the years.

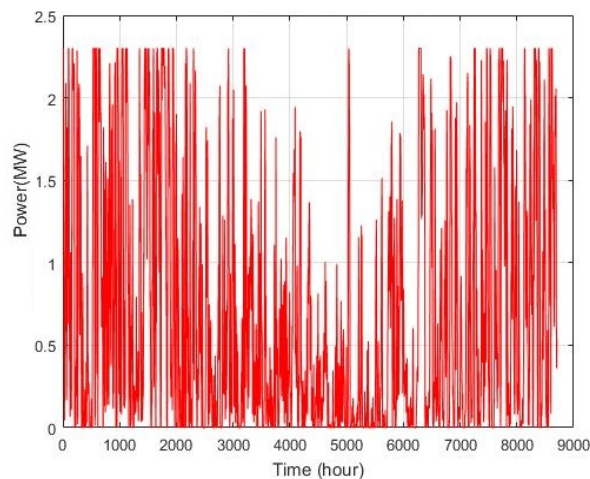
To this point, all the HOEC models expressed good candidacy, while model A shows the best performance in most of the performance evaluation matrices, based on the sizing results achieved using the proposed sizing sequence.

To further ensure the results of HOEC-A, LBESS sizing is carried out using two of the famous optimization algorithms: Particle Swarm Optimization (PSO), and Pattern Search Algorithm (PSA). Results, shown in Table 6, demonstrate the effectiveness of the proposed algorithm, in determining the optimum LBESS parameters, mainly due to its strong analytical component. The results ensure that the wind-wave mix in HOEC A, augmented with LBESS, even with an optimized size determined by the proposed sequence, the PSO or the PSA, is a good candidate to start with for developing a single combined Wind-WEC-LBESS device, in an approach that is like coupling WindWec with Batwind [23] illustrated in Fig. 11.

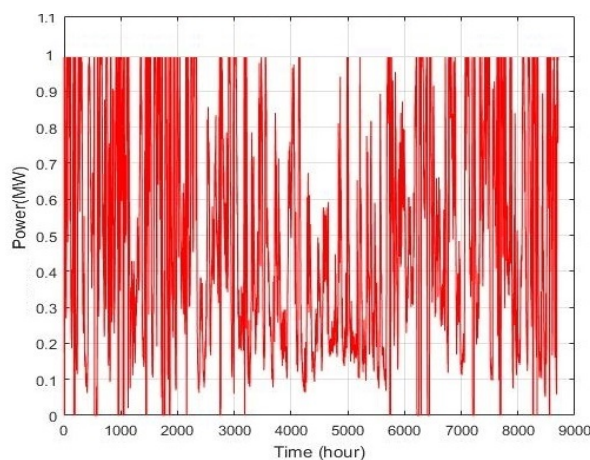
Table 6. LBESS sizes for HOEC-A obtained using the proposed sequence vs PSO and PSA

Method	C_O (MWh)	P_{BO} (MW)
Proposed algorithm	7.3	1.4677
PSO	7.6	1.4714
PSA	7.5999	1.4705

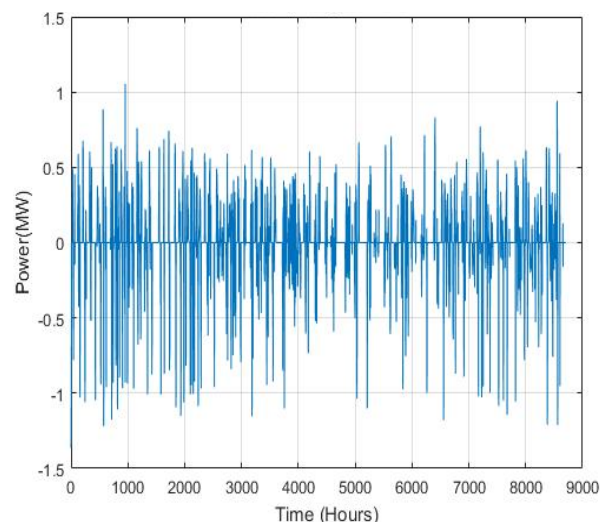
Future work on this Wind-WEC-LBESS synergy includes improving the proposed approach in this research, to include an additional constraint on LBESS weight with respect to the dimensions of the WET and WEC. Further, new RES could be added to the same device.



(a) Extracted power from wind

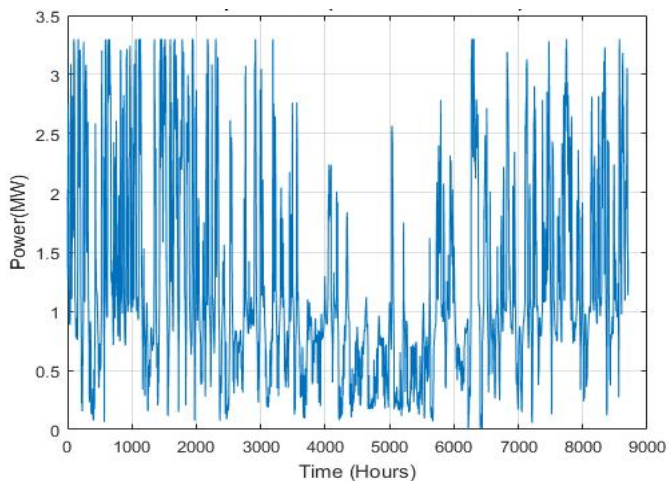


(b) Extracted power from waves

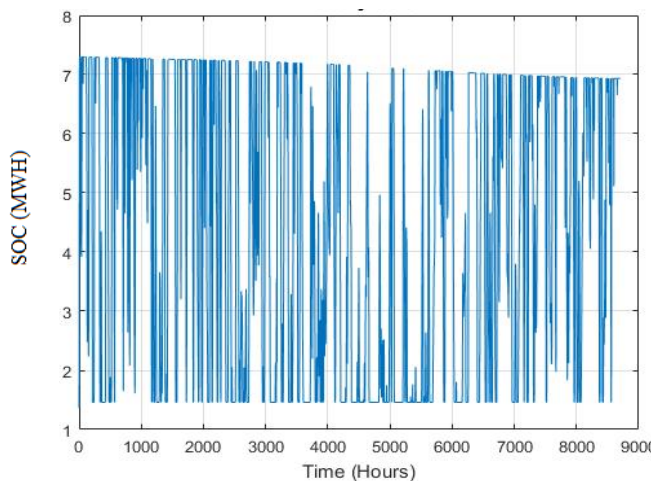


(c) HOEC-A’s LBESS output power

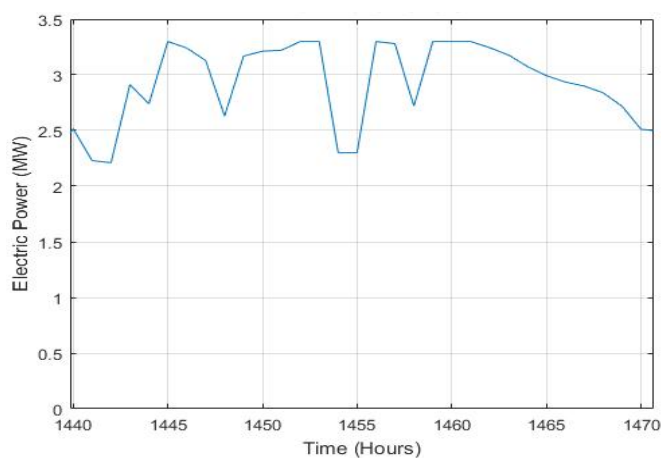
Fig. 8. Individual power production during a year for HOEC-A’s parts (WET, WEC and LBESS).



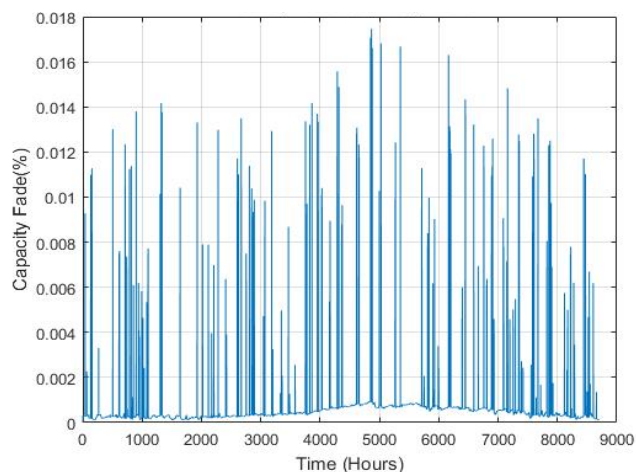
(a) Generated power (P_{REN}) for a year,



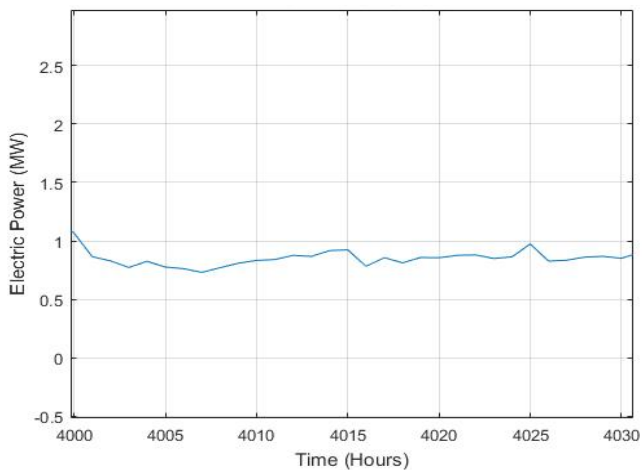
(a) (Maximum) SOC degradation over a year,



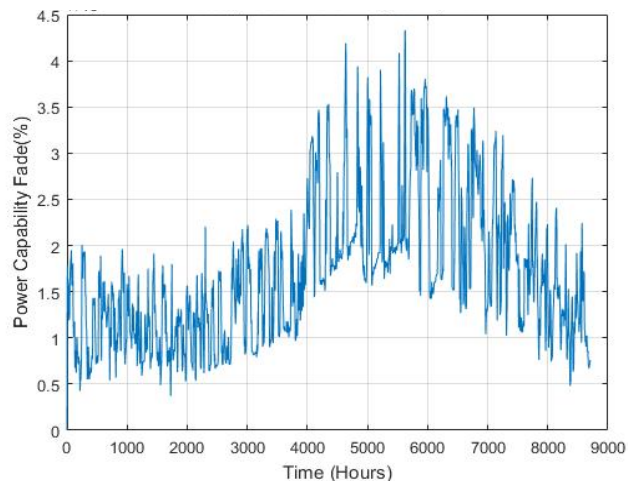
(b) Example for power generated on a winter day which falls on the higher side of energy production.



(b) Total C_{fade}



(c) Example for power generated on a summer day, which falls on the lower side of energy production.



(c) Total PC_{fade} multiplied by 10^{-6} by

Fig. 9. Total generated power curves in the case study for HOEC A.

Fig. 10. One-year-long LBESS performance curves for HOEC A.

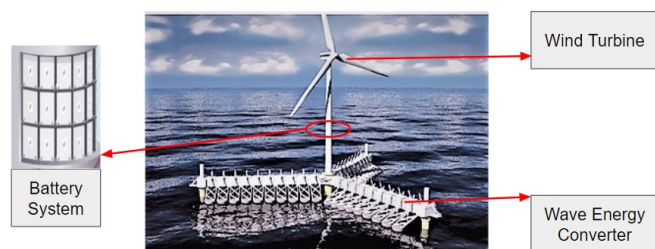


Fig. 11. Illustration for the WWB device, with WET, WEC and LBESS along the vertical axis.

5. Conclusion

In this research, a study on reliability of hybrid renewable Wind-wave system augmented with LBESS for supplying an OOnG load was conducted. LFP/C LBESS was implemented as a solution to enhance power reliability. The LBESS model accounted for capacity and power capability, as well as parameters degradation. A case study with different scenarios was carried out on LOOP location's data. A semi-analytical-semi-iterative search algorithm was designed to find the optimal LBESS size for each case. Results demonstrate the improvement in load level that could be satisfied with a typical combined WWB-HOEC. In the studied location, the improvements (φ - δb) started at 0.93% and were up to 3.11%. LBESS lifetimes hovered around 3.9 years. Finally, the analysis showed models A and C exhibited the best behaviors among the different HOEC models. Simulations showed that the proposed WWB-HOEC concept, regardless of the battery ageing, not only saves area but also provides a good reliability level in an OOnG environment. Besides, for HOEC-A, LBESS optimization results obtained by using the proposed algorithm are validated against those obtained using PSO and GA.

Therefore, integrating such WWB-HOECs could be a key solution for cutting down GHG' emissions from OOnG platforms, and related applications. Future work could include furtherly investigating the WWB HOEC single-device concept, as well as incorporating other RESSs, like floating PV and marine current energies, into HOEC, which will open new research horizons.

References

[1] J. Z. Tee, I. L. H. Lim, K. Zhou and O. Anaya-Lara, "Transient Stability Analysis of Offshore Wind With O&G Platforms and an Energy Storage System," 2020 IEEE Power & Energy Society General Meeting (PESGM), 2020, pp. 1-5, doi: 10.1109/PESGM41954.2020.9281706.

[2] G. Lambert, A. Costabeber, P. Wheeler and Y. R. De Novaes, "A Unidirectional Insulated AC-DC Converter Based on the Hexverter and Multipulse-Rectifier," in IEEE Transactions on Power Electronics, vol. 35, no. 3, pp. 2363-2371, March 2020, doi: 10.1109/TPEL.2019.2928555.

[3] R. N. Fard and E. Tedeschi, "Integration of distributed energy resources into offshore and subsea grids," in CPSS Transactions on Power Electronics and

Applications, vol. 3, no. 1, pp. 36-45, March 2018, doi: 10.24295/CPSSTPEA.2018.00004.

[4] J. Dakic, M. Cheah-Mane, O. Gomis-Bellmunt and E. Prieto Araujo, "HVAC Transmission System for Offshore Wind Power Plants Including Mid-cable Reactive Power Compensation: Optimal design and comparison to VSC-HVDC transmission," in IEEE Transactions on Power Delivery, doi: 10.1109/TPWRD.2020.3027356.

[5] J. J. Valera-García and I. Atutxa-Lekue, "On the Optimal Design of Hybrid-Electric Power Systems for Offshore Vessels," in IEEE Transactions on Transportation Electrification, vol. 5, no. 1, pp. 324-334, March 2019, doi: 10.1109/TTE.2018.2883870.

[6] Q. Li, Y. Mao, Y. Liu, A. Zhang and W. Yang, "Modeling of Integrated Energy System of Offshore Oil and Gas Platforms Considering Couplings Between Energy Supply System and Oil and Gas Production System," in IEEE Access, vol. 8, pp. 157974-157982, 2020, doi: 10.1109/ACCESS.2020.3020135.

[7] E. D. Stoutenburg and M. Z. Jacobson, "Reducing Offshore Transmission Requirements by Combining Offshore Wind and Wave Farms," in IEEE Journal of Oceanic Engineering, vol. 36, no. 4, pp. 552-561, Oct. 2011, doi: 10.1109/JOE.2011.2167198.

[8] X. Zhao, Z. Yan and X. Zhang, "A Wind-Wave Farm System with Self-Energy Storage and Smoothed Power Output," in IEEE Access, vol. 4, pp. 8634-8642, 2016, doi: 10.1109/ACCESS.2016.2631505.

[9] S. D. Ahmed, F. S. M. Al-Ismail, M. Shafiullah, F. A. Al-Sulaiman and I. M. El-Amin, "Grid Integration Challenges of Wind Energy: A Review," in IEEE Access, vol. 8, pp. 10857-10878, 2020, doi: 10.1109/ACCESS.2020.2964896.

[10] "How can an oil company be best at offshore wind?," Equinor, [Online]. Available: <https://www.equinor.com/en/magazine/hywind-oil-industry-expertise.html>. [Accessed 7 5 2021].

[11] F. Taghizadeh-Hesary, & Yoshino, N, "Sustainable solutions for green financing and investment in renewable energy projects. Energies, vol. 13, no. 4, pp. 788, 2020, doi: 10.3390/en13040788.

[12] Hartmann J, Inkpen AC, Ramaswamy K. "Different shades of green: Global oil and gas companies and renewable energy". Journal of International Business Studies, 2020, doi: 10.1057/s41267-020-00326-w

[13] M. L. D. S. A. H. S. David D.J.Taylor, "Black into green: A BIG opportunity for North Dakota's oil and gas producers," Applied Energy, vol. 242, pp. 1189-1197, 15 May 2019.

[14] Q. Li, Y. Mao, Y. Liu, A. Zhang and W. Yang, "Modeling of Integrated Energy System of Offshore Oil and Gas Platforms Considering Couplings Between Energy Supply System and Oil and Gas Production System," in IEEE Access, vol. 8, pp. 157974-157982, 2020, doi: 10.1109/ACCESS.2020.3020135.

[15] Clemente D, Rosa-Santos P, Taveira-Pinto F, "On the potential synergies and applications of wave energy converters: A review". Renewable and Sustainable Energy Reviews, vol. 135, 110162, 2021, doi: 10.1016/j.rser.2020.110162.

- [16] M. A. Syed and M. Khalid, "Moving Regression Filtering with Battery State of Charge Feedback Control for Solar PV Firming and Ramp Rate Curtailment," in *IEEE Access*, vol. 9, pp. 13198-13211, 2021, doi: 10.1109/ACCESS.2021.3052142.
- [17] Qais MH, Hasanien HM, Alghuwainem S. Output power smoothing of wind power plants using self-tuned controlled SMES units. *Electric Power Systems Research*. Vol 178, 106056, 2020, doi: 10.1016/j.epsr.2019.106056.
- [18] Y. Zhang, P. Stansby and G. Li, "Non-causal Linear Optimal Control with Adaptive Sliding Mode Observer for Multi-Body Wave Energy Converters," in *IEEE Transactions on Sustainable Energy*, vol. 12, no. 1, pp. 568-577, Jan. 2021, doi: 10.1109/TSTE.2020.3012412.
- [19] U. Sur, A. Biswas, J. N. Bera and G. Sarkar, "Holomorphic Embedding Power Flow Analysis of Hybrid-Tidal-Farm-Integrated Power Distribution System," in *IEEE Systems Journal*, doi: 10.1109/JSYST.2021.3063624.
- [20] G. Lavidas, and K. Blok, "Shifting wave energy perceptions: The case for wave energy converter (WEC) feasibility at milder resources" *Renewable Energy*, 170, pp.1143-1155, 2021,
- [21] M. Karimirad and K. Koushan, "WindWEC: Combining wind and wave energy inspired by hywind and wavestar," 2016 IEEE International Conference on Renewable Energy Research and Applications (ICRERA), 2016, pp. 96-101, doi: 10.1109/ICRERA.2016.7884433.
- [22] A. R. Aardal, J. I. Marvik, H. Svendsen and J. O. G. Tande, "Offshore Wind as Power Supply to Oil and Gas Platforms," in *Offshore Technology Conference*, 30 April-3 May, Houston, Texas, USA, 2012.
- [23] H. G. Svendsen, M. Hadiya, E. V. Øyslebø and K. Uhlen, "Integration of offshore wind farm with multiple oil and gas platforms," in 2011 IEEE Trondheim PowerTech, Trondheim, Norway, 2011.
- [24] M. Korpås, L. Warland, W. He, J. O. G. Tande, "A case-study on offshore wind power supply to oil and gas rigs," *Energy Procedia*, no. 24, pp. 18-26, 2012.
- [25] H. Lee, S. K. Poguluri and Y. H. Bae, "Performance Analysis of Multiple Wave Energy Converters Placed on a Floating Platform in the Frequency Domain," *Energies*, vol. 11, no. 2, 2018.
- [26] L. Marquis, M. Kramer, J. Kringelum, J. Chozas and N. Helstrup, "Introduction of Wavestar Wave Energy Converters at the Danish offshore wind power plant Horns Rev 2," in 4th International Conference on Ocean Energy, Dublin, 17 to 19 of October 2012.
- [27] Judicael Aubry, Paul Bydlowski, Bernard Multon, Hamid Ben Ahmed, and Bruno Borgarino, "Energy Storage System Sizing for Smoothing Power Generation of Direct Wave Energy Converters," in *ICOE*, Bilbao, Spain, 2010.
- [28] D Friedrich and G Lavidas, "Evaluation of the effect of flexible demand and wave energy converters on the design of Hybrid Energy Systems," *IET Renewable Power Generation*, vol. 11, no. 9, pp. 1113 - 1119, 2017.
- [29] Elisabetta Tedeschi, Jonas Sjolte, Marta Molinas, and Maider Santos, "Stochastic Rating of Storage Systems in Isolated Networks with Increasing Wave Energy Penetration," *Energies*, vol. 6, pp. 2481-2500, 2013.
- [30] Elisabetta Tedeschi, Eider Robles, Maider Santos, Olivier Duperray, and Fernando Salcedo, "Effect of Energy Storage on a Combined Wind and Wave Energy Farm," in *IEEE Energy Conversion Congress & Exposition 1012 (ECCE12)*, 2012.
- [31] M. Yesilbudak and A. Colak, "Integration Challenges and Solutions for Renewable Energy Sources, Electric Vehicles and Demand-Side Initiatives in Smart Grids," 2018 7th International Conference on Renewable Energy Research and Applications (ICRERA), 2018, pp. 1407-1412, doi: 10.1109/ICRERA.2018.8567004.
- [32] D. Buhagiar, Sant, T., Farrugia, R.N., Aquilina, L., Farrugia, D. and Strati, F.M., "Small-scale Experimental Testing of a Novel Marine Floating Platform with Integrated Hydro-pneumatic Energy Storage" *Journal of Energy Storage*, vol. 24, pp.100774, 2019.
- [33] S. d. I. Torre, J. M. González-González, J. A. Aguado and S. Martín, "Optimal battery sizing considering degradation for renewable energy integration," *IET Renewable Power Generation*, vol. 13, no. 4, p. 572 – 577, 2019.
- [34] D. García-Violini, Y. Peña-Sanchez, N. Faedo, C. Windt, F. Ferri and J. V. Ringwood, "Experimental Implementation and Validation of a Broadband LTI Energy-Maximizing Control Strategy for the Wavestar Device," in *IEEE Transactions on Control Systems Technology*, doi: 10.1109/TCST.2021.3052479.
- [35] A. Babarit, J. Hals, M.J. Muliawan, A. Kurniawan, T. Moan and J. Krokstad, "Numerical benchmarking study of a selection of wave energy converters," *Renewable Energy*, vol. 41, pp. 44-63, May 2012.
- [36] "Wave Star energy. Wave Star bølgekraftmaskine 1:40 skala model," [Online]. Available: <http://wavestarenergy.com/sites/default/files/nei-dk-4501.pdf> [Accessed 24 4 2021].
- [37] P. B. Frigaard, T. L. Andersen, J. P. Kofoed, M. M. Kramer and S. Ambühl, "Wavestar Energy Production Outlook," Aalborg: Department of Civil Engineering, Aalborg University. DCE Technical reports, No. 201, 2016.
- [38] NDBC: Adjusted Wind Speeds. [Online]. www.ndbc.noaa.gov/adjust_wind.shtml
- [39] M. Ebrahimi, M. Rastegar, M. Mohammadi, A. Palomino and M. Parvania, "Stochastic Charging Optimization of V2G-Capable PEVs: A Comprehensive Model for Battery Aging and Customer Service Quality," in *IEEE Transactions on Transportation Electrification*, vol. 6, no. 3, pp. 1026-1034, Sept. 2020, doi: 10.1109/TTE.2020.3005875.
- [40] P. Mouratidis, B. Schüßler and S. Rinderknecht, "Hybrid Energy Storage System consisting of a Flywheel and a Lithium-ion Battery for the Provision of Primary Control Reserve," 2019 8th International Conference on Renewable Energy Research and Applications (ICRERA), 2019, pp. 94-99, doi: 10.1109/ICRERA47325.2019.8996553.
- [41] D. I. Stroe, "Lifetime Models for Lithium-ion Batteries used in Virtual Power Plant Applications," PhD Thesis, Aalborg University, 2014.

- [42] P. Mouratidis, B. Schüßler and S. Rinderknecht, "Hybrid Energy Storage System consisting of a Flywheel and a Lithium-ion Battery for the Provision of Primary Control Reserve," 2019 8th International Conference on Renewable Energy Research and Applications (ICRERA), 2019, pp. 94-99, doi: 10.1109/ICRERA47325.2019.8996553.
- [43] Askarzadeh, "Electrical power generation by an optimised autonomous PV/wind/tidal/battery system," IET Renewable Power Generation, vol. 11, no. 1, pp. 152-164, 2017.
- [44] E. S. Jones, H. Gong and D. M. Ionel, "Optimal Combinations of Utility Level Renewable Generators for a Net Zero Energy Microgrid Considering Different Utility Charge Rates," 2019 8th International Conference on Renewable Energy Research and Applications (ICRERA), 2019, pp. 1014-1017, doi: 10.1109/ICRERA47325.2019.8996529.
- [45] Y. Mizuno, Y. Tanaka, F. Kurokawa and N. Matsui, "A Hospital Grid with Renewable Energy System Applied to Virtual Power Plant," 2020 8th International Conference on Smart Grid (icSmartGrid), 2020, pp. 203-207, doi: 10.1109/icSmartGrid49881.2020.9144796.
- [46] I. M. Opedare, T. Adekoya, A. Longe, "Optimal Sizing of Hybrid Renewable Energy System for off-Grid Electrification: A Case Study of University of Ibadan Abdusalam Abubakar Post Graduate Hall of Residence," International Journal of Smart Grid, vol. 4, no. 4, pp. 176-189, 2020.